

Edge-Oriented Phosphatizing Engineering of 2D Ni-MOFs with tailored d-band Center for Boosting the Catalytic Activity

Chongchong Wang,^{[a][b]} Lulu Kong,^[b] Bingbing Chen,^[c] Lin Zhou,^{ [b]} Wei Wang,^{*}*

^{[a][b]} Shaohua Wei^{ [a][b]}*

[a] School of Chemistry and Chemical Engineering, Yancheng Institute of Technology.

Yancheng 224051, China.

[b] College of Chemistry and Materials Science, Jiangsu Key Laboratory of Bio-functional Materials, Jiangsu Collaborative Innovation Centre of Biomedical Functional Materials, Key Laboratory of Applied Photochemistry, Nanjing Normal University.

Nanjing 210023, China.

[c] Department of Energy Science and Engineering, Nanjing Tech University.

Nanjing 210009, China.

E-mail: zhoulin@njnu.edu.cn, wangw@ycit.edu.cn, shwei@njnu.edu.cn

1. Experimental Details

1.1. Materials

N-N-Dimethylacetamide (DMAC), chloroform (CHCl₃), ethyl alcohol absolute, and sodium borohydride (NaBH₄) were all obtained from Sinopharm Chemical Reagent (Shanghai, China). Nickel (II) acetate tetrahydrate (NiC₄H₆O₄·4H₂O), p-phthalic acid

(1,4-H₂BDC), sodium hypophosphite monohydrate (NaH₂PO₂•H₂O), and 4-nitrophenol (4-NP) were procured from Aladdin (Shanghai, China). The water used in all experiments was double distilled water.

1.2. Instruments

The transmission electron microscope (TEM) images were performed on H-7650 microscopy (Hitachi, Japan) operating at 80 kV. High-resolution TEM (HRTEM), high-angle annular dark field scanning TEM (HAADF-STEM) images and selected area electron diffraction (SAED) analysis were performed with a Talos F200S G2 transmission electron microscope with an accelerating voltage of 200 kV (Thermo Fisher, USA), equipped with EDS detectors. X-ray diffraction (XRD) pattern was collected with an X-ray Powder Diffractometer (Rigaku Corporation, Japan). UV-vis spectrum was carried out using a Cary 50 spectrophotometer (Varian, USA). X-ray photoelectron spectroscopy (XPS) was recorded on an ESCALAB X-ray Microprobe (Thermo Fisher, USA). Thermogravimetric analysis (TGA) measurement was carried out in N₂ at a heating rate of 10 °C min⁻¹ using a thermogravimetric analyzer (Perkin-Elmer, USA). N₂ sorption measurements were conducted on ASAP 2020 instrument. The FTIR spectrums were obtained on the Fourier transform infrared spectrometer (Cary-5000, Varian, USA). The contents of nickel and phosphorus were measured by inductively coupled plasma atomic emission spectrometer (ICP, Prodigy, USA). Mass spectra were determined by a MS-ESI (Agilent, USA).

1.3. Density functional theory (DFT) calculations

We have employed the Vienna Ab Initio Package (VASP) to perform all the DFT calculations within the generalized gradient approximation (GGA) using the PBE formulation.^{1,2} The projected augmented wave (PAW) potentials were used to describe the ionic cores,³ take valence electrons into account using a plane wave basis set with a kinetic energy cutoff of 450 eV. Partial occupancies of the Kohn-Sham orbitals were allowed using the Gaussian smearing method and a width of 0.05 eV. The electronic energy was considered self-consistent when the energy change was smaller than 10^{-5} eV. A geometry optimization was considered convergent when the force change was smaller than 0.05 eV/Å. Grimme's DFT-D3 method was used to describe the dispersion interactions.³ The Brillouin zone integral uses the surfaces structures of $1 \times 1 \times 1$ monkhorst pack K-point sampling. Finally, the adsorption energies (E_{ads}) are calculated as $E_{ads} = E_{ad/sub} - E_{ad} - E_{sub}$, where $E_{ad/sub}$, E_{ad} and E_{sub} are the optimized adsorbate/substrate system, the adsorbate in the structure and the clean substrate respectively. The free energies were obtained by $G = E_{total} + E_{ZPE} - TS$, where E_{total} , E_{ZPE} , and TS are the ground-state energy, zero-point energies, and entropy terms, respectively, with the latter two taking vibration frequencies from DFT.

2. Results and Discussion

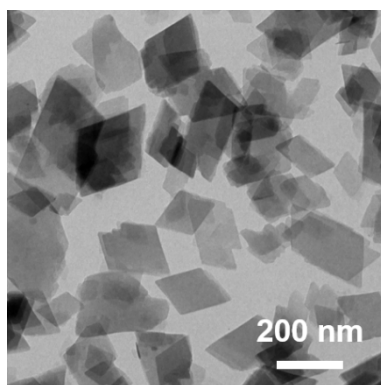


Figure S1. The TEM image of 2D Ni-MOF.

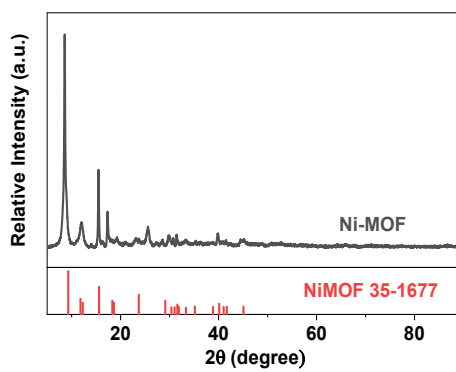


Figure S2. The XRD pattern of 2D Ni-MOF.

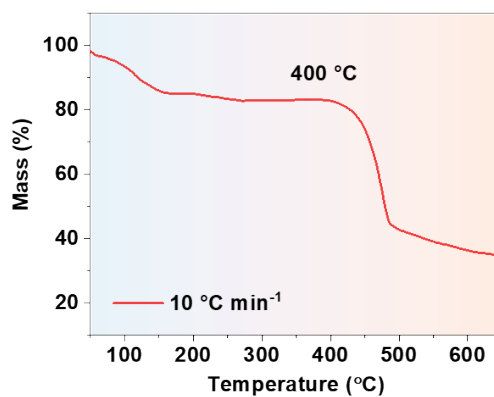


Figure S3. The TGA curve of 2D Ni-MOF.

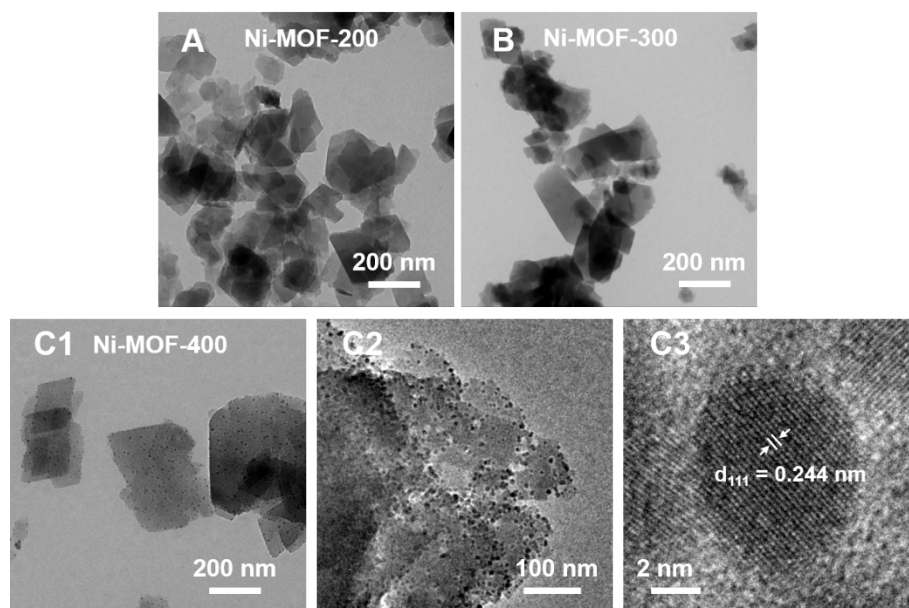


Figure S4. The TEM images of 2D Ni-MOF after carbonization at 200 °C (A), 300 °C (B) and 400 °C (C1, C2). The HRTEM image of 2D Ni-MOF after carbonization at 400 °C (C3).

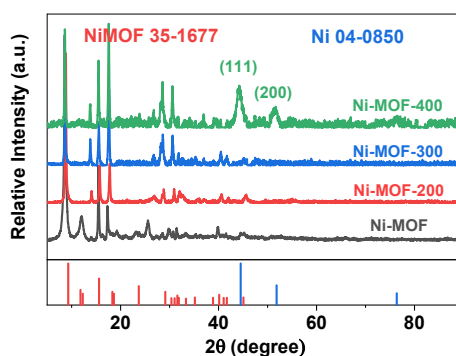


Figure S5. The XRD patterns of 2D Ni-MOF after carbonization at different temperatures.

In order to preserve the structure of Ni-MOF as much as possible during the pyrolysis process, the effect of pyrolysis temperature on Ni-MOF was determined, and the thermogravimetric curve was first obtained (Figure S3). The rapid weight loss

occurred at 400 °C, indicating that the structure of Ni-MOF is significantly damaged. Therefore, the pyrolysis temperature should be controlled below 400 °C. The pyrolysis behavior was also confirmed by TEM. As shown in Figure S4A and Figure S4B, the Ni-MOF maintained their parallelogram-like shape with smooth surface under 200 °C and 300 °C in argon atmosphere. After annealing at 400 °C, a large number of nanoparticles appeared on the surface of Ni-MOF (Figure S4C), HRTEM (Figure S4C) and XRD patterns (Figure S5) proved that these nanoparticles were Ni. Which indicating that when the pyrolysis temperature reaches 400 °C, the structure of Ni-MOF has been destroyed.

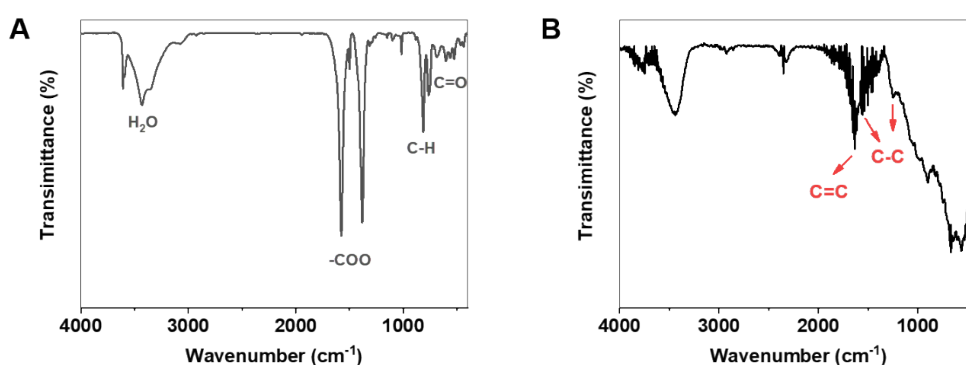


Figure S6. The FTIR spectrum of 2D Ni-MOF (A) and Ni-MOF-400P (B).

FTIR spectra of the as-prepared 2D Ni-MOFs are shown in Figure S6, the stretching vibration bands around 3200-3500 cm^{-1} belong to H_2O molecules, which proving the existence of coordinated H_2O molecules in the 2D Ni-MOF. The two intensive peaks at around 1575.9 cm^{-1} and 1382.2 cm^{-1} are attributed to the asymmetric stretching vibration and symmetric stretching vibration of terephthalate anions ($-\text{COO}$),

respectively. The peaks at 815.8 cm^{-1} and 758.1 cm^{-1} are characteristic of the p-aromatic C-H stretch peaks. The peak centered at 525.3 cm^{-1} corresponding to C=O group.^{4, 5}

Moreover, XRD data (Figure 1C) show that Ni-MOF-400P has been carbonized, C-C peak and C=C peak which attributed to amorphous carbon can be found in the corresponding FT-IR spectrums (Figure 1B, Figure S6B).⁶

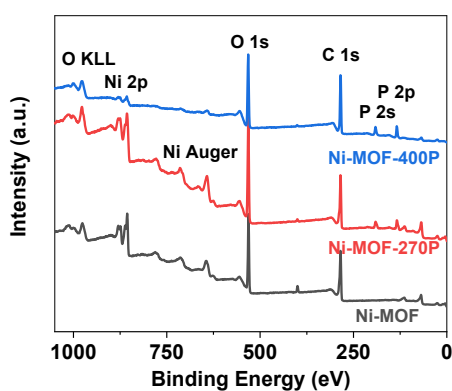


Figure S7. The survey XPS spectra of 2D Ni-MOF, Ni-MOF-270P and Ni-MOF-400P.

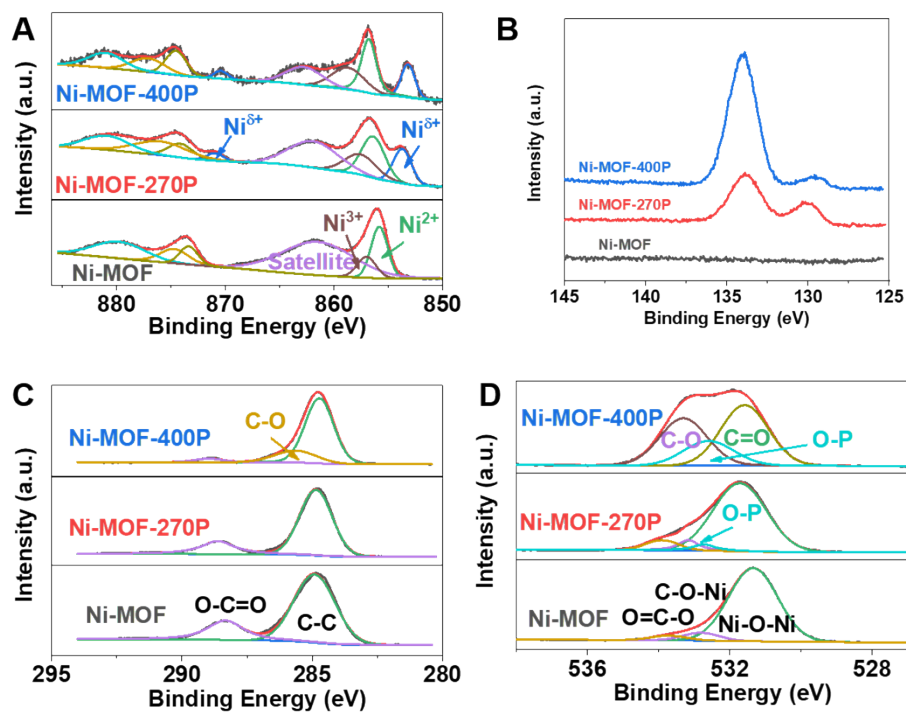


Figure S8. (A) The Ni 2p XPS spectra of 2D Ni-MOF, Ni-MOF-270P and Ni-MOF-400P. (B) The P 2p XPS spectra of 2D Ni-MOF, Ni-MOF-270P and Ni-MOF-400P. (C) The C 1s XPS spectra of 2D Ni-MOF, Ni-MOF-270P and Ni-MOF-400P. (D) The O 1s XPS spectra of 2D Ni-MOF, Ni-MOF-270P and Ni-MOF-400P.

XPS was conducted to study the surface elemental composition and valence of the products after Ni-MOF phosphating. Ni 2p, C 1s, and O 1s were observed in the wide-survey scan XPS spectra of all samples (Figure S7), and it was worth noting that strong P 2p peaks appeared after phosphating treatments. The Ni 2p XPS spectra (Figure S8A) for Ni-MOF show three couples of subpeaks at about 855.83 and 857.01 eV, 861.49 and 873.37 eV, 874.72 and 879.80 eV, assigned to Ni²⁺, Ni³⁺, and the corresponding satellite peaks, respectively.⁷ The binding energies at 853.7 eV (Ni 2p_{3/2}) and 870.94 eV (Ni 2p_{1/2}) are in accordance with Ni^{δ+} for Ni₂P after phosphating at 270 °C.⁸ As for

the high resolution XPS P 2p spectra (Figure S8B), the peak at 129.85 eV can be ascribed to $P^{\delta-}$ in Ni_2P , whereas the other peak at 133.95 eV is associated with oxidized P species.⁹ The C 1s XPS spectra (Figure S8C) contains two different types of carbon at 284.95 eV and 288.45 eV attribute to C-C and O-C=O bonds from terephthalate in the Ni-MOF.⁷ C-O peak appears at 285.61 eV after phosphating at 400 °C, with the disappearance of O-C=O bond. In the O 1s XPS spectra (Figure S8D), the peaks at 531.34, 532.81, and 533.72 eV are indexed as Ni-O-Ni, C-O-Ni, and O=C-O, respectively.⁷ It is worthwhile mentioning that a new sub-peak binding at 532.65 eV appeared after phosphating, which can be indexed to the O-P.^{10, 11} These all proves the formation of Ni-MOF/ Ni_2P heterostructure.

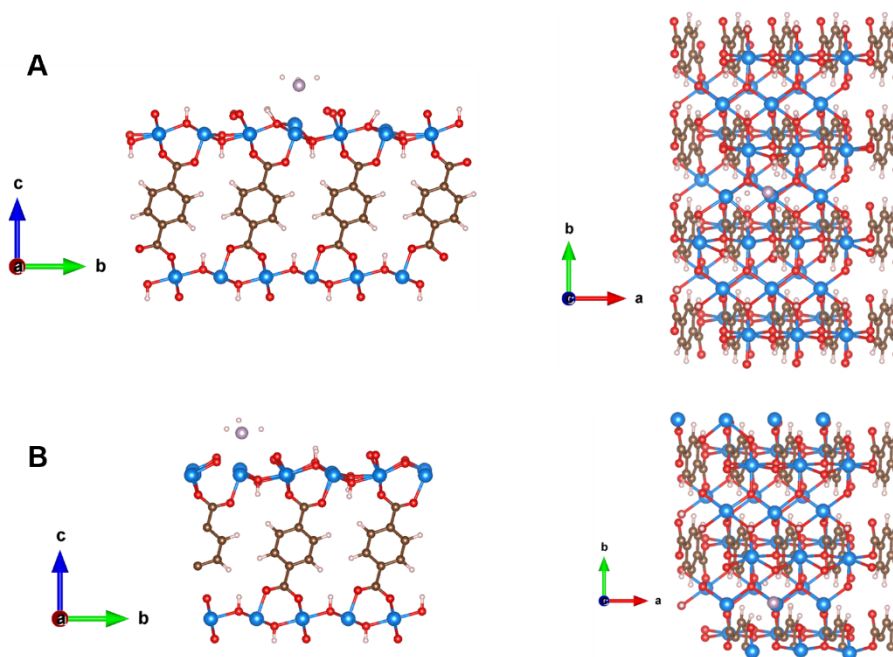


Figure S9. (A) Top and side views of the adsorption of PH_3 molecule on the basal of Ni-MOF. (B) Top and side views of the adsorption of PH_3 molecule on the edge of Ni-MOF. The visualization of crystal structure is realized by VESTA software. The Ni, C,

O, P and H atoms are denoted as blue, brown, red, purple and white spheres, respectively.

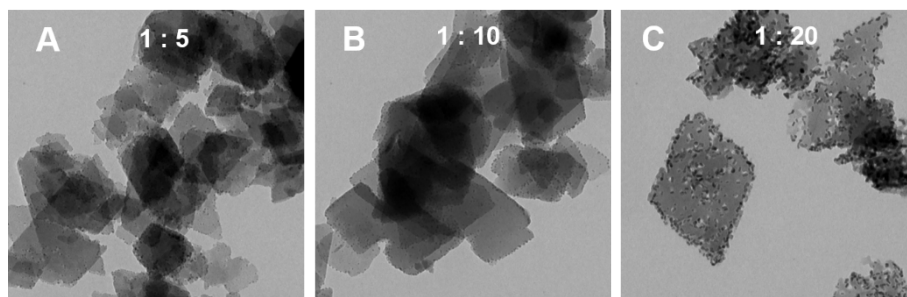


Figure S10. The TEM images of 2D Ni-MOF by changing the content of NaH_2PO_2 under the same phosphating temperature.

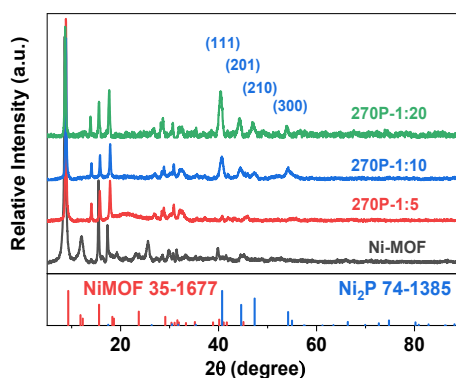


Figure S11. The XRD patterns of 2D Ni-MOF by changing the content of NaH_2PO_2 under the same phosphating temperature.

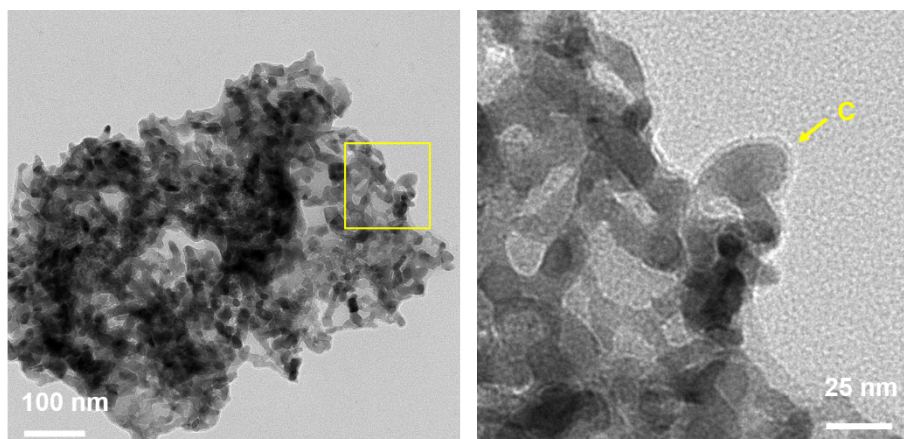


Figure S12. The TEM image of Ni-MOF-400P, the carbon layer on the surface is clearly visible.

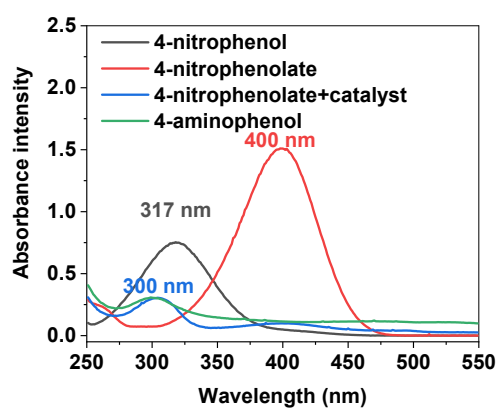


Figure S13. The UV-vis spectra for the solution of 4-AP, 4-NP, 4-nitrophenolate anions and the reaction solution in the reduction of 4-NP to 4-AP catalyzed by Ni-MOF-270P at room temperature.

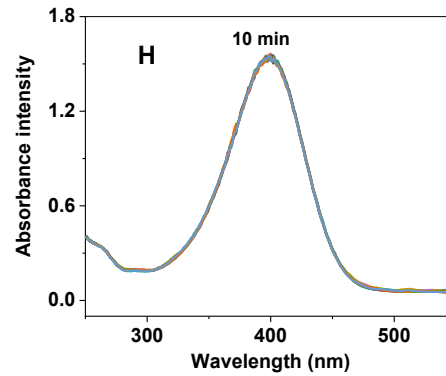
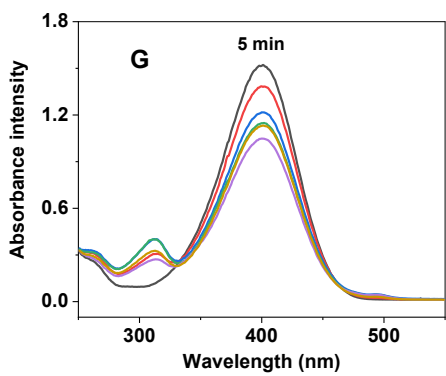
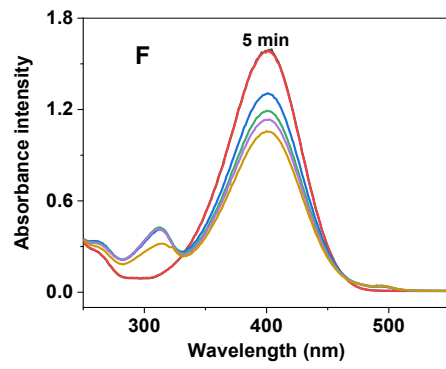
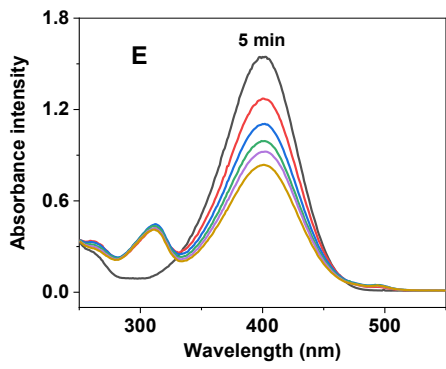
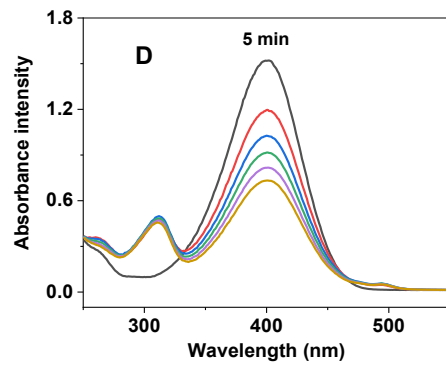
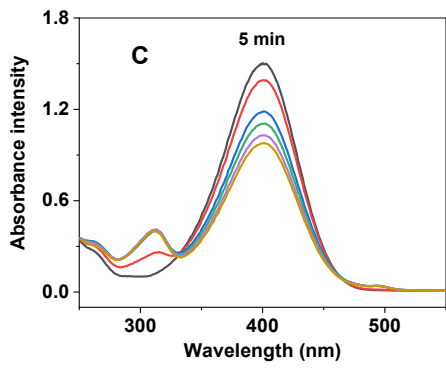
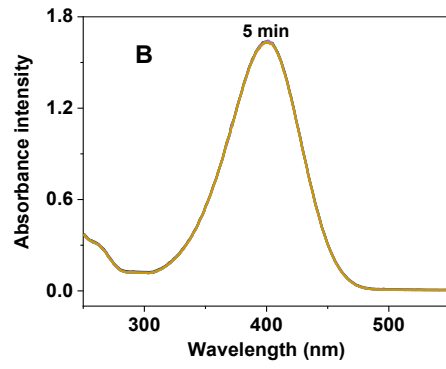
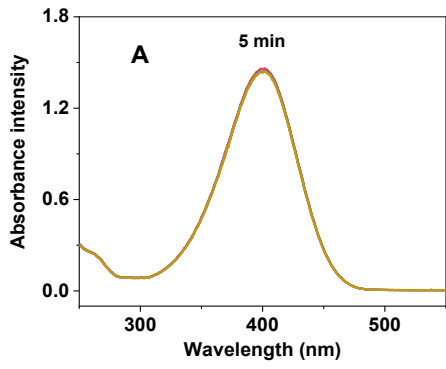


Figure S14. UV-vis absorption spectra of 4-NP reduced to 4-AP by NaBH_4 in the present of Ni-MOF-200P (A), Ni-MOF-250P (B), Ni-MOF-260P (C), Ni-MOF-270P (D), Ni-MOF-280P (E), Ni-MOF-300P (F), Ni-MOF-400P (G), and without catalysts (H) at a certain time interval. The concentrations of the catalysts were $1.25 \mu\text{g mL}^{-1}$.

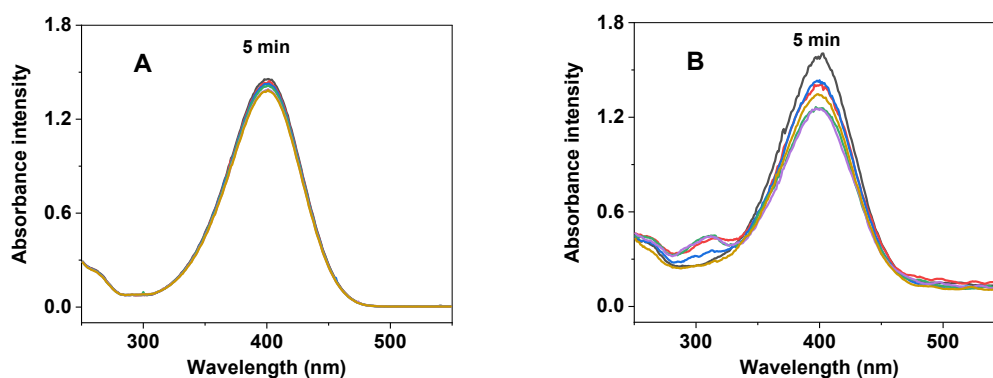


Figure S15. UV-vis absorption spectra of 4-NP reduced to 4-AP by NaBH_4 in the present of 10% Pd/C ($2.5 \mu\text{g mL}^{-1}$, A) and 20% Pt/C ($1.25 \mu\text{g mL}^{-1}$, B) at a certain time interval.

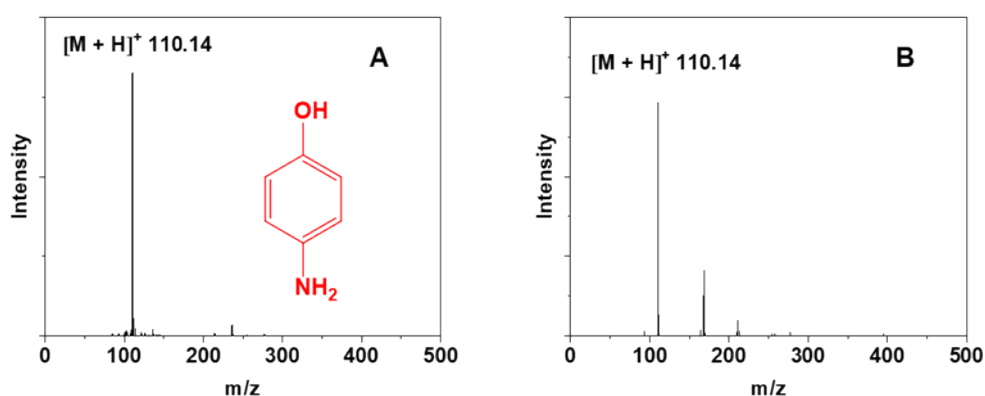


Figure S16. The mass spectrums for 4-AP (A) and the product in the reduction of 4-NP to 4-AP catalyzed by Ni-MOF-270P at room temperature (B).

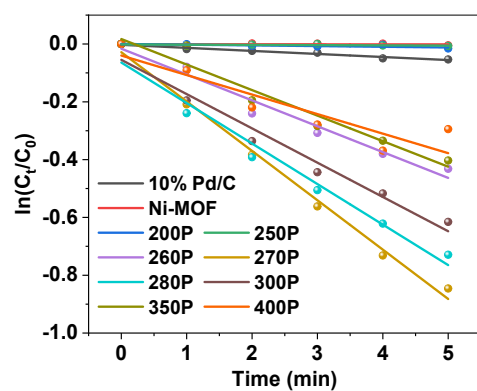


Figure S17. Pseudo-first order kinetic plots of 4-NP reduction catalyzed by the catalysts.

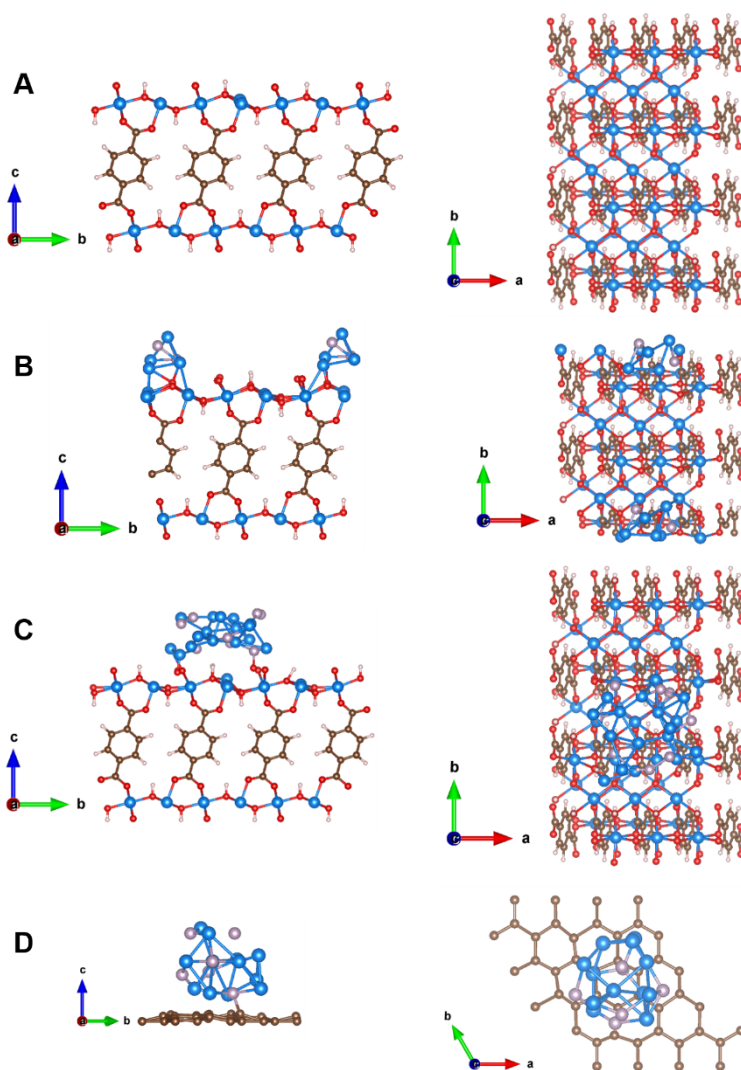


Figure S18. (A) Top and side views of Ni-MOF. (B) Top and side views of Ni-MOF/Ni₂P edge (Ni₂P is distributed at the edges of Ni-MOF). (C) Top and side views of Ni-MOF/Ni₂P basal (Ni₂P is distributed at the basal of Ni-MOF). (D) Top and side views of C/Ni₂P. The visualization of crystal structure is realized by VESTA software. The Ni, C, O, P and H atoms are denoted as blue, brown, red, purple and white spheres, respectively.

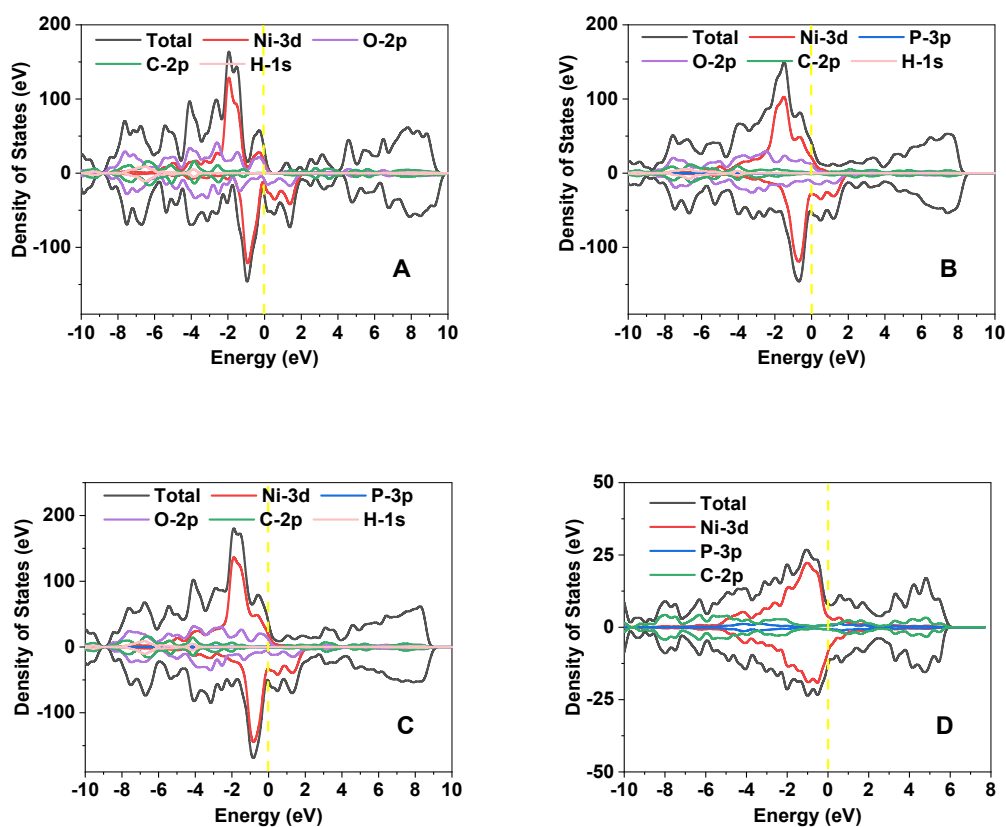


Figure S19. Total density of states (DOS) and partial density of states (PDOS) diagrams of Ni 3d, P 3p, O 2p, C 2p and H 1s orbitals in the Ni-MOF (A), Ni-MOF/Ni₂P edge (B), Ni-MOF/Ni₂P basal (C), and C/Ni₂P (D) models.

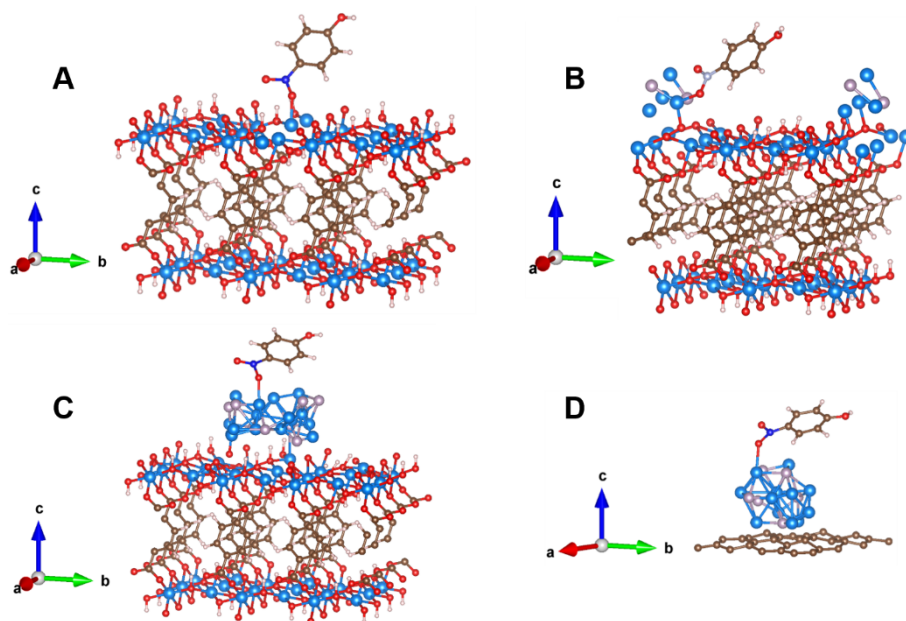


Figure S20. Adsorption models of 4-NP on Ni-MOF (A), Ni-MOF/Ni₂P edge (B), Ni-MOF/Ni₂P basal (C), and C/Ni₂P (D). The visualization of crystal structure is realized by VESTA software. The Ni, C, O, P and H atoms are denoted as blue, brown, red, purple and white spheres, respectively.

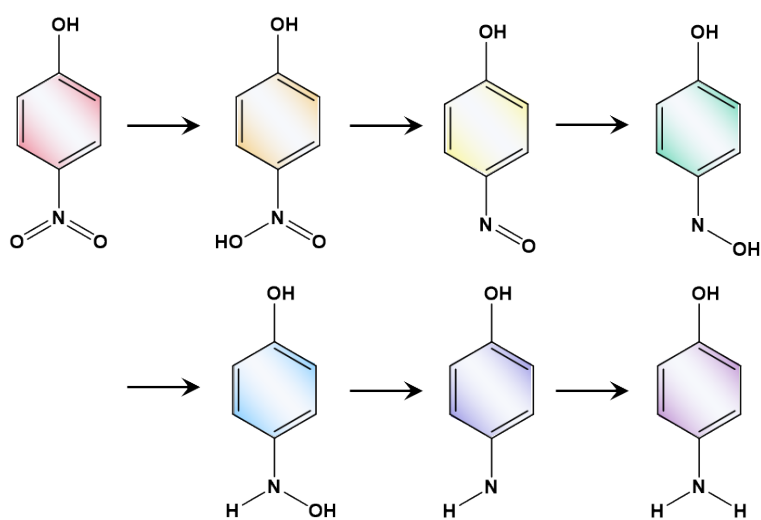


Figure S21. Schematic diagram of the reaction pathways of 4-NP on the catalysts.

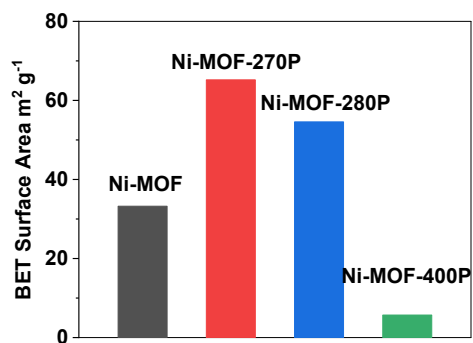


Figure S22. The BET surface area of 2D Ni-MOF, Ni-MOF-270P, Ni-MOF-280P and Ni-MOF-400P.

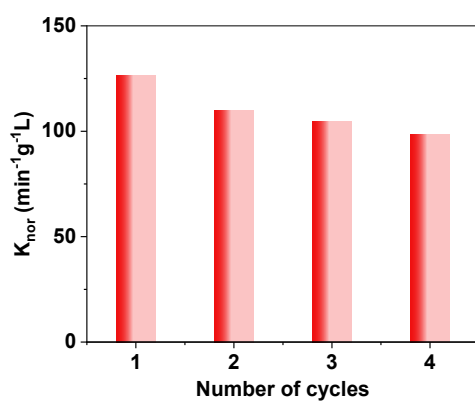


Figure S23. Cycling performance of Ni-MOF-270P for 4-NP reduction.

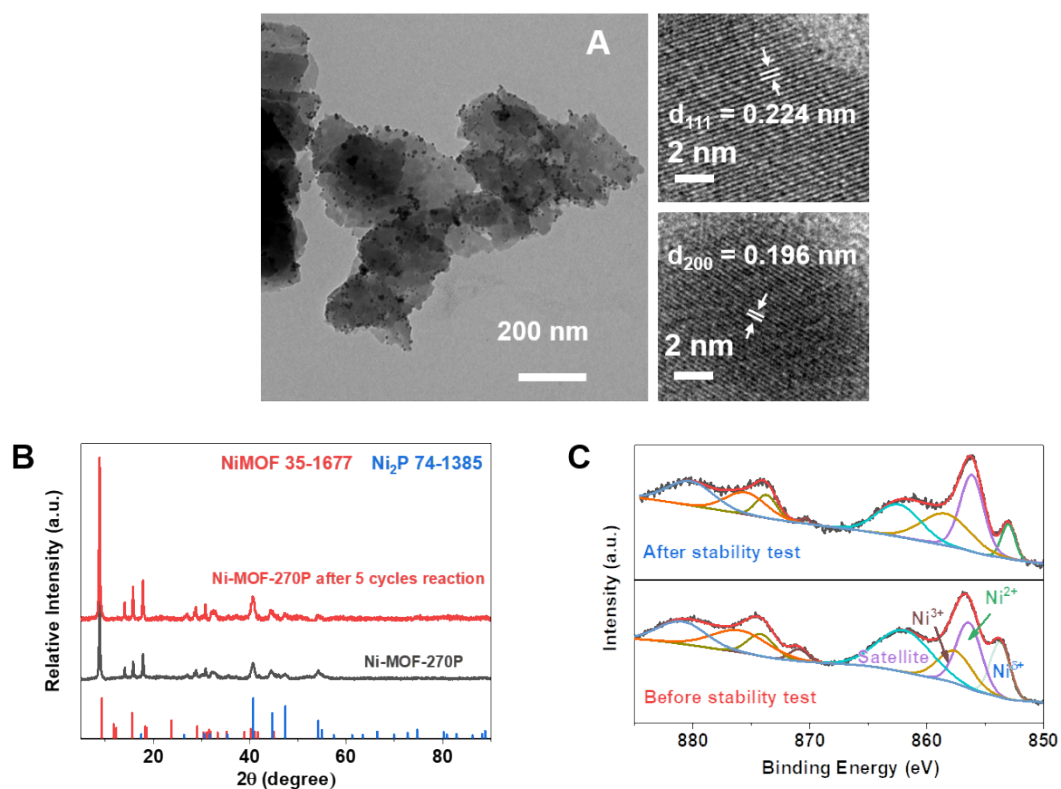


Figure S24. The TEM (A), XRD patterns (B) and XPS spectra comparison of Ni-MOF-270P before and after the stability test.

Table S1. Comparison of the catalytic activities of various metal-based materials for 4-NP reduction.

Catalyst	Amount of catalyst (mg/L)	Amount of 4-NP (mmol/L)	Metal content (wt %)	TOF ^a (mmol g ⁻¹ min ⁻¹)	Reference
Co ₃ O ₄ /HN Ts	33.33	0.12	11.95	0.27	[45]
DE/Ni/N-C-800	1000	0.17	21.82	0.51	[46]
fcc-Ni/Gr	17.24	0.14	46.60	4.35	[47]
fcc/hcp-Ni/Gr	17.24	0.14	58.10	9.20	[47]
BNNF-Cu	125.00	0.072	0.40	16.11	[33]

Ni-MOF-270P	1.25	0.075	33.68	14.85	This work
Au/g-C ₃ N ₄ -6	20.00	0.072	6.00	5.99	[48]
AgPd NCS/rGO	20.00	0.14	76.70	3.04	[49]
AgNPs/Si NSs	200	0.12	10.43	8.63	[50]
Ni@Cu@Pd	3.60	0.071	100	6.53	[51]
Ag _{0.5} -Cu _{0.5} NPs@PZS	35.71	0.061	1	24.29	[52]
Au-Rh@SiO ₂	19	0.057	7.9	22.65	[53]

^a TOF: The amount of reactant that is converted into product per minute by 1 g of metal.

TOF = the amount of consumed 4-NP (mmol) / the mass of the metal in catalyst (g) / reaction time (min).

References

- 1 J. P. Perdew, K. Burke and M. Ernzerhof, *Phys. Rev. Lett.*, 1998, **77**, 3865-3868.
- 2 P. Giannozzi, O. Andreussi, T. Brumme, O. Bunau, M. Buongiorno Nardelli, M. Calandra, R. Car, C. Cavazzoni, D. Ceresoli, M. Cococcioni, N. Colonna, I. Carnimeo, A. Dal Corso, S. de Gironcoli, P. Delugas, R. A. DiStasio, A. Ferretti, A. Floris, G. Fratesi, G. Fugallo, R. Gebauer, U. Gerstmann, F. Giustino, T. Gorni, J. Jia, M. Kawamura, H. Y. Ko, A. Kokalj, E. Kucukbenli, M. Lazzeri, M. Marsili, N. Marzari, F. Mauri, N. L. Nguyen, H. V. Nguyen, A. Otero-de-la-Roza, L. Paulatto, S. Ponce, D. Rocca, R. Sabatini, B. Santra, M. Schlipf, A. P. Seitsonen, A. Smogunov, I. Timrov, T. Thonhauser, P. Umari, N. Vast, X. Wu and S. Baroni, *J. Phys. Condens Matter.*, 2017, **29**, 465901.
- 3 S. Grimme, J. Antony, S. Ehrlich and H. Krieg, *J. Chem. Phys.*, 2010, **132**, 154104.

- 4 S. Rezaee and S. Shahrokhian, *Appl. Catal. B: Environ.*, 2019, **244**, 802-813.
- 5 Y. Wang, Y. Liu, H. Wang, W. Liu, Y. Li, J. Zhang, H. Hou and J. Yang, *ACS Appl. Energy Mater.*, 2019, **2**, 2063-2071.
- 6 V. Tucureanu, A. Matei and A. M. Avram, *Crit. Rev. Anal. Chem.*, 2016, **46**, 502-520.
- 7 M. Wang, Y. Xu, C. K. Peng, S. Y. Chen, Y. G. Lin, Z. Hu, L. Sun, S. Ding, C. W. Pao, Q. Shao and X. Huang, *J. Am. Chem. Soc.*, 2021, **143**, 16512-16518.
- 8 C. Tang, R. Zhang, W. Lu, Z. Wang, D. Liu, S. Hao, G. Du, A. M. Asiri and X. Sun, *Angew. Chem. Int. Ed.*, 2017, **56**, 842-846.
- 9 T. Sun, S. Zhang, L. Xu, D. Wang and Y. Li, *Chem. Commun. (Camb)*, 2018, **54**, 12101-12104.
- 10 H. Liu, S. Zhu, Z. Cui, Z. Li, S. Wu and Y. Liang, *Nanoscale*, 2021, **13**, 1759-1769.
- 11 R. Wang, X. Y. Dong, J. Du, J. Y. Zhao and S. Q. Zang, *Adv. Mater.*, 2018, **30**, 1703711.